



# Machinability of nickel-titanium shape memory alloys under dry and chilled air cutting conditions

Zainal Abidin Zailani<sup>1,2</sup> · Paul Tarisai Mativenga<sup>3</sup>

Received: 21 July 2022 / Accepted: 3 April 2023 / Published online: 24 April 2023  
© The Author(s) 2023

## Abstract

Nickel-titanium (NiTi) shape memory alloys (SMAs) undergo phase transformation between austenitic and martensitic phases in response to applied thermal or mechanical stress, resulting in unique properties and applications. However, machinability often becomes challenging due to property and temperature sensitivity attributes. The use of chilled air to influence machinability in macro-milling was investigated in this study. Other than that, differential scanning calorimetry (DSC) was used to determine the temperature of phase transformation. The results showed that milling with chilled air and minimal lubrication significantly improved machining performance by reducing tool wear and burr formation. Moreover, surface quality has also improved significantly. A notable discovery is that the machining process can change the critical conditions for phase transition, enabling new performance capability of tuning material hysteresis.

**Keywords** Shape memory alloys · Milling · Sustainable machining · Chilled air · Minimum quantity lubrication

## 1 Introduction

In addition to being ductile, NiTi SMAs, also known as nominal 55-nitinol (55 wt. % Ni), exhibit “mechanical memory” as a function of deformation and temperature [1]. SMAs are smart materials that can return to their original form or shape when subjected to heat, stress, or a magnetic field [2]. Also, they exhibit reversible diffusionless phase transitions, resulting in unique properties and applications.

These properties, along with their extra advantages of biocompatibility, high ductility, high strength-to-weight

ratio, good fatigue and corrosion resistance, and high damping capacities, make NiTi-based alloys functional for novel applications. Apart from that, applications could be based on free recovery, constrained recovery, actuator capability, and superelasticity. The temperature range for the martensite-to-austenite transformation influences the performance of NiTi SMAs for a specific application. Note that this is critical in deciding on an actuator [3].

To fully realize the application of SMAs, manufacturing processes for these materials must be further developed. Milling is widely used in most manufacturing process chains for ordinary materials such as metals, ceramics, and composites and allows for greater dimensional accuracy, higher surface finish, complex shapes, and a wide range of batch sizes. Due to high ductility, temperature sensitivity, and strong work hardening in machining, these materials are difficult to machine, as NiTi alloy causes difficulty in chip breaking and burr control [4]. At the same time, rapid tool wear [5] renders the machinability of the material. The material’s high strength causes additional mechanical loading on the tool-workpiece interface, resulting in strong adhesion on the tool flank face [6]. It was discovered that the longer the cutting time, the more the adhesion of the workpiece material to the cutting tool [7]. In addition, [8] support this contention by highlighting the poor quality of the workpiece and excessively high tool wear even when cutting parameters

---

Zainal Abidin Zailani and Paul Tarisai Mativenga contributed equally to this work.

---

✉ Zainal Abidin Zailani  
zailani@unimap.edu.my

Paul Tarisai Mativenga  
P.Mativenga@manchester.ac.uk

<sup>1</sup> Faculty of Mechanical Engineering Technology, Universiti Malaysia Perlis, 02600 Arau, Perlis, Malaysia

<sup>2</sup> Sustainable Manufacturing Technology Research Group, Faculty of Mechanical Engineering Technology, Universiti Malaysia Perlis (UniMAP), 02600 Arau, Perlis, Malaysia

<sup>3</sup> Department of Mechanical, Aerospace and Civil Engineering, The University of Manchester, Manchester M13 9PL, UK

have been optimized. Due to high tool flank wear, only a narrow range of cutting parameters are applicable [9].

The machinability of NiTi is, in fact, more difficult in comparison with other engineering materials. A review of the literature shows the majority of research on NiTi had been conducted on dry cutting [8], minimum quantity lubricant (MQL) [4], and cryogenic cooling [10]. The effects of cryogenic cooling on machining performance measures were recently studied comprehensively for numerous materials as well as NiTi. It was ascertained that this system contributed to improved machining performance [11]. However, the main concern about this machining technology is related to the initial costs of system setup, which requires additional equipment not provided with machine tools and frequent refills of liquid nitrogen [12]. A relatively new technique that employs cooling air has generated interest among researchers, with this system seeming an appropriate substitute for cryogenic cooling. Furthermore, many studies have indicated that this system helps enhance tool life and cutting performance [13].

Phase transformation adds another critical aspect and variability to machinability due to three dissimilar crystal structures, namely twinned martensite, detwinned martensite, and austenite [14]. When heated, NiTi alloy undergoes a transformation from martensite to austenite. The austenite phase is quite hard and has a much-sophisticated Young's modulus. Martensite, on the other hand, has a very low yield strength and is easily deformed into a new form [15]. It can thus be inferred those changes in temperature and deformation during machining significantly affect the material and its machinability. Machining the material in its martensite form would be more favorable compared to the austenite phase. A previous study reported that cryogenic machining of martensite NiTi led to lower force as compared to machining the preheated work material [16]. On the contrary, a study revealed that machining NiTi under the martensitic phase led to higher force and tool wear due to the martensite phase's ductility and tensile strength [17]. When the sample was heated above the austenite start phase temperature, the phase was changed and became harder for the machine. Moreover, thicker burrs were created under the machining of martensitic alloy compared to austenitic alloy [9].

The literature review leads to the conclusion that changes in temperature and deformation during machining may have a significant impact on the material's machinability and phase transition. Therefore, better machinability performance would result from machining the material in its martensite form with less deformation. Additionally, it is anticipated that this research will add to our fundamental knowledge and understanding of the relationship between the stress that materials are subjected to during cutting processes and how that stress affects material behavior, particularly transformation hysteresis. For the purpose of choosing

a material for a specific application, this characteristic is crucial.

Other than that, temperature-driven phase transformation and temperature sensitivity present a major scientific challenge for the machining of NiTi alloy material. Therefore, phase transformation temperatures determine whether chilled air would be suitable for avoiding phase transitions in NiTi. The research hypothesis was that effective cooling provided by chilled air systems could reduce heat produced at the tool-workpiece interface, keep the workpiece material in its easier-to-cut martensitic process, and improve the machinability of NiTi SMAs. Again, the aim for the chilled air, in this case, was to control the workpiece temperature that was very sensitive to phase transition and not the tool, which the machinist normally applies. These findings could be beneficial to be applied to other temperature-sensitive materials, which are also influenced by phase transformation temperature. To ascertain this hypothesis, cutting tests were established.

## 2 Materials and methods

### 2.1 Workpiece material characterization

The workpiece material designated for this research was a NiTi alloy supplied by American Element USA. The composition of the alloy was confirmed by energy dispersive X-ray analysis (EDXA) to be 55 wt% nickel and 45 wt% titanium. The workpiece dimensions were 70 mm in length, 20 mm in width, and 15 mm in height.

The material transformation temperatures were measured using DSC. This would be useful in determining its phase at room temperature and the critical temperature at which it would transform. A sample 2.0-mm long by 2.0-mm wide and 1.0-mm-thick NiTi was tested using a TA Instrument Q100 DSC. The procedure required each specimen to be first cleaned with alcohol, dried, and placed in an aluminium pan. Subsequently, this pan was concealed, sealed, and put in a DSC machine. The sample was then subjected to a heating–cooling–heating cycle with heating and cooling temperatures set between  $-90\text{ }^{\circ}\text{C}$  and  $160\text{ }^{\circ}\text{C}$ . The amount of heat released and absorbed during the phase transition was recorded according to the temperature. The total time for the entire test cycle was 77 min, with the ramp rate set at  $10\text{ }^{\circ}\text{C}$  per minute.

The temperatures for the start of the transformation to austenite, the end of the transformation to austenite, the start of the transformation to martensite, and the end of the transformation to martensite were plotted in a calorimetric diagram at  $50\text{ }^{\circ}\text{C}$ ,  $69\text{ }^{\circ}\text{C}$ ,  $35\text{ }^{\circ}\text{C}$ , and  $14\text{ }^{\circ}\text{C}$ , respectively, as shown in Fig. 1. These values were critical for studying phase transformations and establishing critical

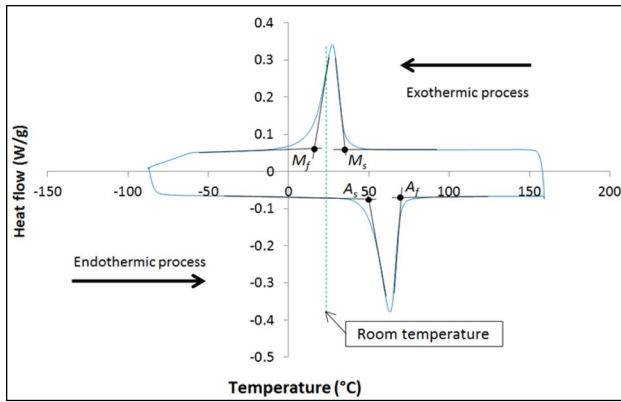


**Fig. 1** Phase transformation temperatures of nickel-titanium (55:45 wt %) shape memory alloy in the as-received form

transformation temperatures. In Fig. 1, these points are illustrated by the intersection points of the tangents to the curve at the phase transformation points. Here, it is indicated that the material was in the martensite phase at room temperature. In this particular circumstance, using chilled air was a more cost-effective and convenient way to avoid phase transition (austenite phase).

First, each sample was mounted on carbon conductive black using compression-mounting resin for microstructure analysis to ease the grinding and polishing process and provide better specimen edge retention for further analysis. The as-received sample was ground with three different grits of abrasive paper (600, 1200, and 2400) and then polished with a diamond slurry monocrystalline paste (6, 3, and 1 micron) to obtain a mirror-like surface. The sample was subsequently etched for 10–20 s using a solution of 3.2% hydrofluoric acid, 14.6% nitric acid, and 82.2% de-ionized water, as recommended by [5]. Serious safety precautions were required because hydrofluoric acid and nitric acid could cause severe burn wounds, eye injuries, and even death. Here, microstructures were imaged using a Keyence VHX-5000 digital microscope. The intercept method, as specified by the ASTM E112 standard for equiaxed or single-phase grain structure, was used to quantify the grain size [18]. Nano-indentation on an MTS nanoindenter XP tester with a load of 5 mN and a penetration depth of 400 nm was used in the vicinity of the subsurface-machined zone to determine the work hardening effect. Load and hardness calibration were done using a fused silica reference. For machined surface strain measurement, an X-ray diffraction Bruker D8 Discover instrument was used.

## 2.2 Experimental setup and machining conditions

Milling experiments were carried out on a Mikron HSM 400 high-speed machining center. The cutting tools used

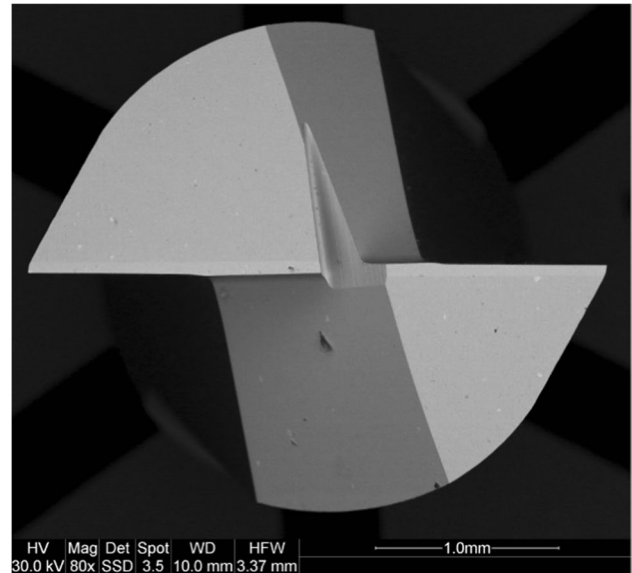


**Fig. 2** Fine grain solid carbide straight cut-end mills

were TiSiN-coated 2-flute fine grain solid carbide straight-cut straight cut-end mills with a diameter of 3.0 mm, as shown in Fig. 2. A tool with a zero-rake angle was selected to strengthen the cutting edge. All tools were imaged with a FEI Quanta 200 SEM to look for flaws in their geometry and cutting-edge radius feature. The tools' average cutting-edge radii were 2.6  $\mu\text{m}$ .

Cutting dry with chilled air as well as chilled air simultaneously applied with MQL was studied. A cutting velocity of 48 m/min, feed per tooth of 0.05 mm, and depth of cut of 0.18 mm were used, as confirmed by pilot tests. Note that five 15-mm-long slots were milled sequentially with a 20% tool diameter stepover. Each test was carried out three times with different and new cutting tools.

A VORTEC adjustable cold air gun, Model 610BSP, as shown in Fig. 3, was utilized to produce temperatures of between  $-9$  and  $-11$   $^{\circ}\text{C}$  at a flow velocity of 13 m/s. It was also equipped with a magnetic base and microfilter. Before cutting, the chilled air was applied to the workpiece for 10 min to stabilize the workpiece temperature. Apart from that, the chilled air temperature was measured using a FLUKE 53II single-input digital thermometer. For air velocity, a PCE-THA 10 thermo-hygro-anemometer was used. The chilled air was directly applied to the workpiece to regulate the temperature. The nozzle was located 15 mm from the tool engagement point on the workpiece and at a  $60^{\circ}$  angle to the spindle axis.

A three-component Kistler Mini-Dynamometer Type 9256C, DAQ system Type 5697A1, and Type 5070A charge amplifier were used to evaluate the cutting forces. The sampling frequency was 5000 Hz with the spindle speed set at 5000 rpm, whereby 60 data points were



Fig. 3 A VORTEC adjustable cold air gun

recorded per tool revolution. The natural frequency for  $F_x$ ,  $F_y$ , and  $F_z$  of the dynamometer was  $\sim 4.0$ ,  $4.8$ , and  $4.6$  kHz, respectively. Meanwhile, the cutting temperature was measured using a FLIR Thermo Vision<sup>TM</sup> A40 thermal camera. Black matte paint was applied to fix the emissivity of the workpiece surface, and a Keyence VK-X200K 3D laser scanning microscope was used to quantify burr size and surface roughness. Lastly, tool wear was examined from scanning electron microscope (SEM) images and Image J software.

### 3 Results and discussion

#### 3.1 Temperature

Because phase transition is directly related to temperature, cutting temperature greatly impacts the machinability of temperature-sensitive materials like NiTi. Figure 4 illustrates the temperature of the tool-workpiece contact area. Lower temperatures were obtained with the presence of the chilled air system. Note that there was a 36% decrease in cutting temperature compared to dry conditions. Based on the DSC curve in Fig. 1, it is proven that convective heat transfer from the chilled airflow was effective in minimizing heat accumulation throughout the cutting process and keeping the workpiece below the austenite start temperature of  $50^\circ\text{C}$ . Additionally, air velocity may be useful to remove chips and metal particles from the cutting region.

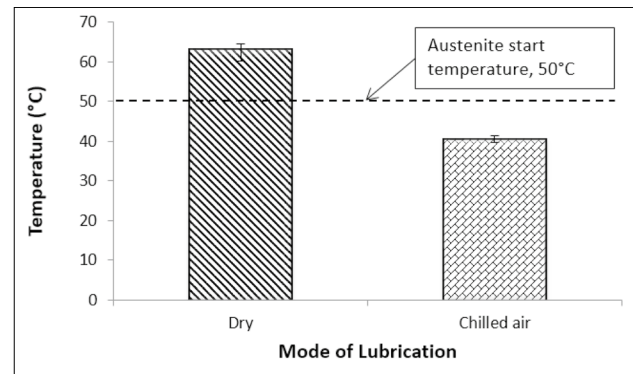


Fig. 4 Workpiece temperature under dry and chilled air cutting

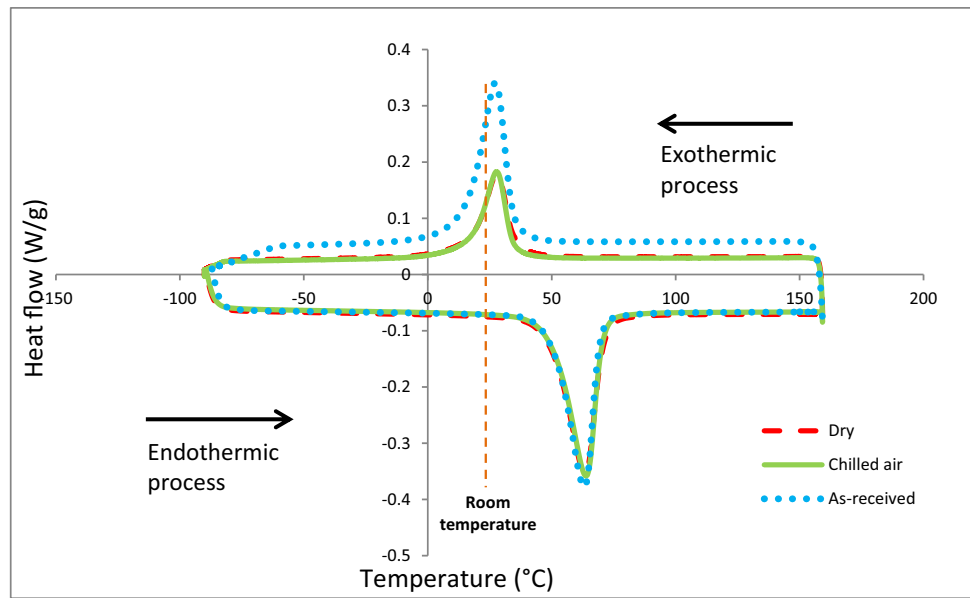
#### 3.2 Differential scanning calorimetry (DSC)

Figure 5 portrays the DSC response of the as-received, dry-cut, and chilled air-cut specimens. A DSC assessment of the machined surface and subsurface accurately determines NiTi alloy machining-induced phase transformation temperatures. It is critical to know whether the machining process subjected the investigated specimen to any stresses, deficiencies, or dislocation density. Here, it had something to do with the cold work phenomenon, which changes the machined surface microstructure.

From the calorimetric diagrams, a difference in the response of the machined specimens and as-received material was observed. The temperatures for the martensite start and martensite finish were shifted. The machining process caused peak narrowing for the transformation from austenite to martensite (i.e., an upper loop of the curve) and subsequently modified the hysteresis. This property is essential in selecting the material for a specific purpose. Apart from that, a small hysteresis is requisite for fast actuation and strongly influences the power consumption needed for the process. Notably, the composition of materials, thermos-mechanical process, and working environment (e.g., applied stress) affect the transformation hysteresis. Machined specimens showed that temperature hysteresis was slightly reduced compared to the as-received specimen. The decrease in transformation temperatures could be ascribed to the creation of residual stress and dislocation density caused by the machining process compared to the as-received specimen. Additionally, Fig. 5 demonstrates that the machining process reduced the specific energy required for austenite to martensitic transformation (lower top peak loop). Therefore, it points to the possibility of decreasing the energy consumption of the actuator for selected applications. The actuation response rate and energy requirements could be modified through machining to provide a new process window and capability for tuning SMAs. Moreover, this



**Fig. 5** DSC response of as-received and machined samples



study indicates that machined surface and subsurface have different phase transformation responses compared to as-received material.

### 3.3 Microstructure analysis

Microstructure analysis was focused on the machined slot end sides below the slot floor. The grain sizes were measured using the linear intercept method. The average grain sizes of the sub-surface machined area in relation to the cutting conditions are shown in Fig. 6. There were no significant alterations between the as-received and chilled air results, except in the dry cutting condition. The average grain sizes for as-received, dry, and chilled air were measured at 25,

43, and 22  $\mu\text{m}$ , respectively. Under dry-cutting conditions, the grains were coarser than those presented in as-received and chilled air conditions. Consequently, there will be more dislocations within the grains. Thus, a lower applied stress is needed to generate a high local stress to cause the grain boundary to collapse. In terms of machinability, a coarser grain size could lead to a bad surface finish, especially for high-ductility materials. Interestingly, a chilled air system helps retain the grain size of the material to be as close as possible to the input condition.

A difference in the thickness of the grain boundaries was noted between as-received and machined specimens. From the EDXA results of the microstructure in Fig. 7 (a), (b), and (c), the dendritic structure in the darker area precipitated

**Fig. 6** Average grain size for as-received material and after dry cutting and cutting in chilled air

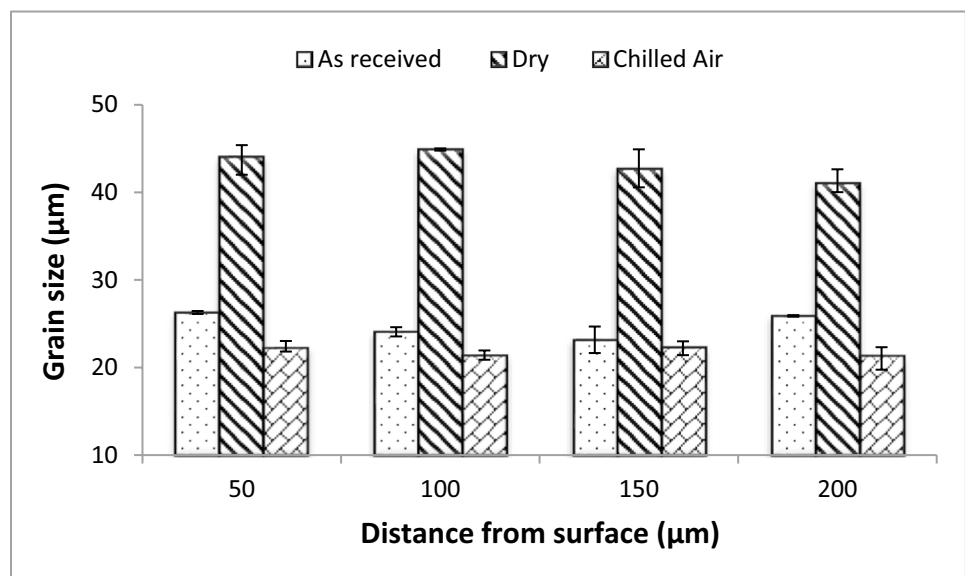
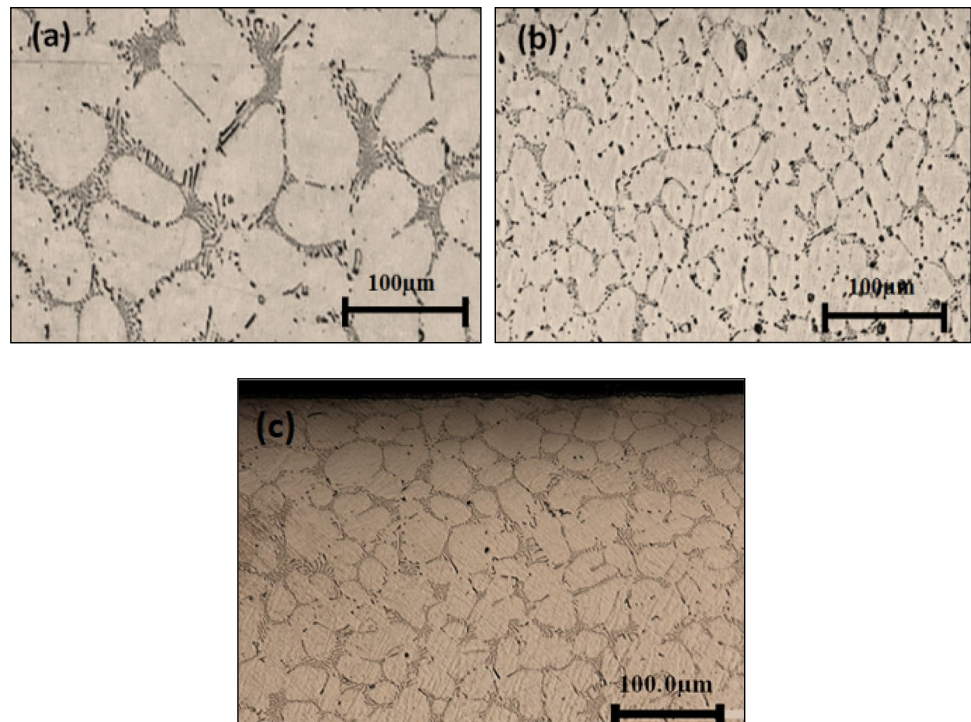


**Fig. 7** Grain boundary in **a** dry cutting **b** chilled air cutting, and **c** as-received



from the grain boundary during dry cutting was richer in titanium than the bulk grain. Note that grain boundaries are areas where the atoms along the boundaries are packed less efficiently and more chaotically. This zone has lower energy than the atoms in the lattice within the grains, ensuring they can be easily removed or chemically bonded to another atom. In addition, this region becomes rougher when subjected to corrosive environments or the etching process.

### 3.4 Nanohardness and surface strain

Work hardening or strain hardening is one of the factors contributing to NiTi's poor machinability. The nano-hardness value was evaluated using various machining conditions to identify the subsurface-affected layer zone. Other than that, the distances from the depth direction were fixed at 10, 20, 30, 40, and 50  $\mu\text{m}$  for each measurement along the cross-section of a milled slot. The formation of new dislocations multiplies during plastic deformation, increasing the dislocation density in the NiTi. The resistance of other dislocations to dislocation motion becomes more constrained as dislocation density rises, making the metal stronger and harder.

Figure 8 depicts the machined subsurface-hardened zone. Here, different trends were visible in the layer of machined components that were affected. When machining in dry conditions, especially when closer to the cutting edge, higher hardness wear was attained. Hence, the higher hardness makes cutting more challenging and accelerates tool wear. The findings are consistent with the tool flank wear and

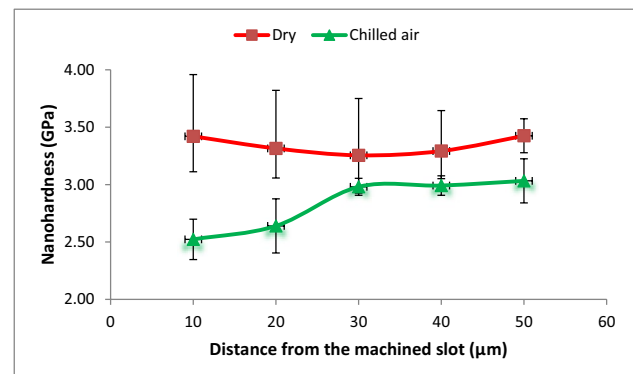


**Fig. 8** Machined surface-hardened zone

burr formation, where a dull tool indicates that ploughing is occurring and that the cutters are not removing the material but rather pushing it to the slot side to create burrs. In addition, the worn tool produces more compressive residual stress than the sharp cutting tool.

Additionally, an X-ray diffraction instrument was used to identify strains from the machined surface. A brief pre-scan was conducted to select the 2-theta range with respect to approximate patterns found for NiTi-type materials from the International Centre for Diffraction Data (ICDD) database. Cobalt radiation was utilized for scanning and to measure the surface strains; measurements were made on the bottom of slots that had been machined. Table 1 compares the machined

**Table 1** Surface strain in as-received and machined samples

| Component              | Strain value |
|------------------------|--------------|
| 1. As received         | 0.0035       |
| 2. Dry cutting         | 0.0056       |
| 3. Chilled-air cutting | 0.0049       |

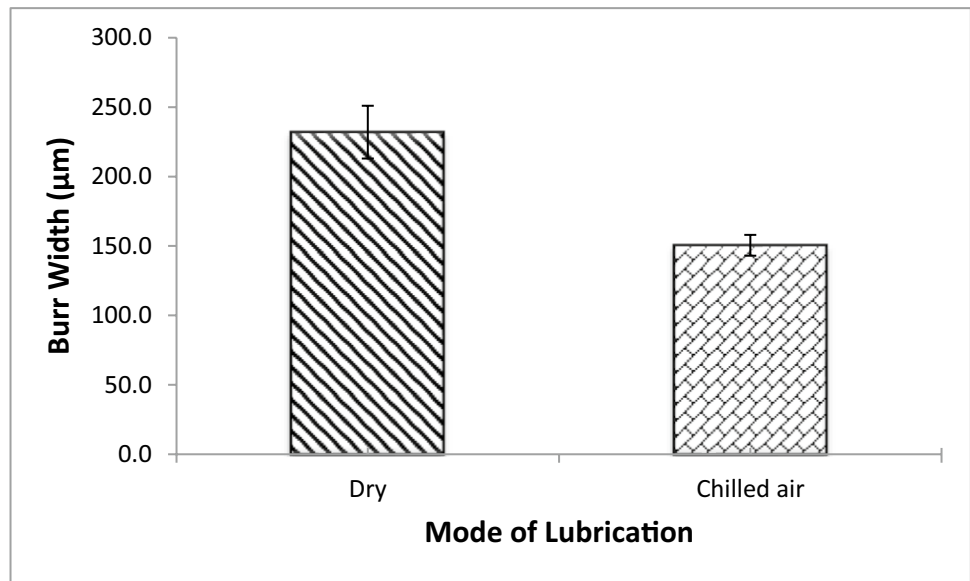
surface’s strain value to the material as received. The strain value was increased under both conditions: dry and chilled air cutting than it was with the as-received material. Under dry cutting, a higher strain value was obtained. This is anticipated to rise along with the amount of cold work occurring in the surface layers. The main cause of this occurrence may be the increase of tool wear that occurs during dry cutting.

### 3.5 Burr formation

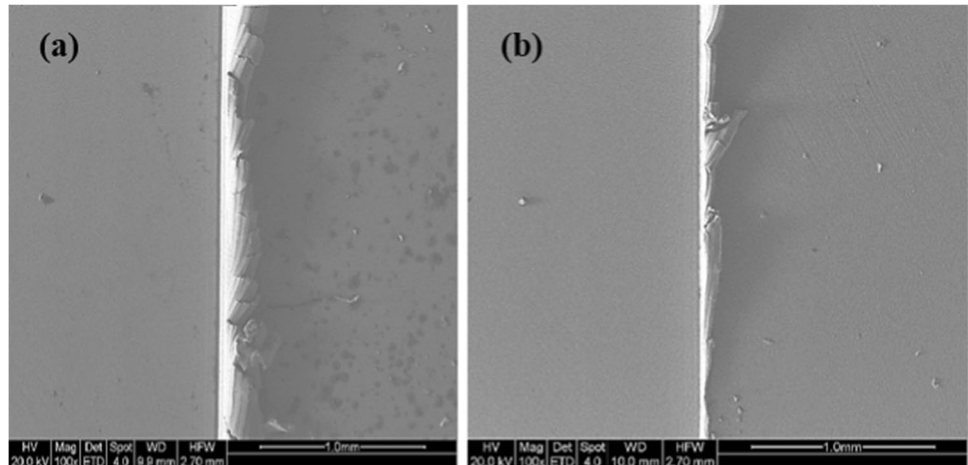
Because of its high ductility and tendency to harden when deformed, burr formation is a significant issue in the machinability of NiTi alloys. Figure 9 illustrates the results of burr formation. According to the findings, burrs were still being produced under chilled-air conditions, albeit in smaller sizes. Burr formation could not be completely eliminated because of its high ductility. Thus, top burrs were the most dominant burr in this experiment. Note that wider top burrs are obtained under dry cutting.

Figure 10 demonstrates the various burr characteristics observed under SEM. The shapes were bent under dry cutting, while chilled-air cutting revealed torn along the edge. This was mainly because burrs produced by the chilled-air system were softer and simpler to remove than the stiffer and more difficult burrs produced by dry cutting.

**Fig. 9** Comparison of average burr width under different cutting conditions



**Fig. 10** Burr formation under **a** Dry cutting and **b** Chilled air cutting



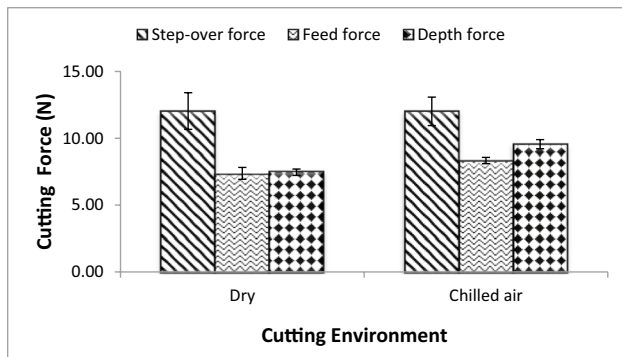


Fig. 11 Variation of forces with cutting environments

### 3.6 Cutting forces

During machining, force in the stepover direction ( $F_x$ ), force in the feed direction ( $F_y$ ), and force in the depth direction ( $F_z$ ) were measured. Figure 11 portrays the forces with the most dominant forces measured in the stepover direction. The other differences were not significant. However, underfeed and depth force, the chilled air gave slightly higher force due to the malleability of the material, which was expected to be under the martensite phase. As a result, it has higher tensile strength and breaking elongation, needing extra force to deform.

### 3.7 Improving surface roughness

NiTi is broadly used in biomedical, aerospace, and other areas where the surface finish of the end product is vital. However, when chilled-air systems were used, the lubricating function was not adequately addressed. Hence, to further improve the machining performance, chilled air and MQL were applied instantaneously in milling tests. For MQL, 100% green Coolube® 2210 cutting lubricant was chosen with the MQL flow rate set at 45 ml/h. Figure 12 presents the surface roughness values obtained.

It is clear that surface roughness could be improved using chilled air instead of dry cutting. This is due to the control or avoidance of transformation from martensite to austenite. Furthermore, the surface roughness in machining NiTi alloys could be further reduced by simultaneously using chilled air and MQL. Other than that, the graph indicates that using a lower feed per tooth improves surface roughness. The machinability of NiTi alloys in terms of the surface finish produced could thus be significantly improved (50% reduction) by the combined use of chilled air and MQL and by exploiting the size effect in machining.

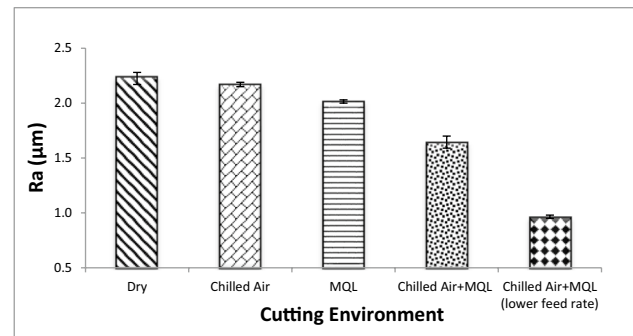


Fig. 12 Roughness average variations between dry, chilled air, MQL, and chilled air applied concurrently with MQL (all experiments done at 0.049 mm/tooth and lower feed rate of 0.010 mm/tooth)

### 3.8 Tool wear

After milling five consecutive slots with a 20% stepover, SEM images were used to quantify the tool wear modes. To reveal each cutting-edge feature, the tools were imaged from the flat bottom face. From Fig. 13 (a), it is obvious that the cutting-edge shape remained round when cutting under chilled air, and flank wear was relatively uniform. In contrast, chipping and a more chamfered edge occurred under dry cutting, as shown in Fig. 13 (b). The average flank wear after machining is presented in Fig. 14. This exhibits that chilled air reduces the average wear and leads to more uniform wear, attributing to the theory that under dry conditions, high temperatures transform to austenite, a more difficult-to-machine phase. Thus, it precipitates higher tool wear.

## 4 Conclusions

This research was conducted to investigate the machining performance of NiTi SMAs. Due to their high ductility and temperature sensitivity, NiTi SMAs are hard to machine mechanically. Apart from that, controlling cutting temperature is one possible solution to this machinability issue. Because the martensite phase is more machinable than austenite in this type of alloy, chilled air keeps the material in the easier-to-cut phase. Moreover, the likelihood of chilled air being suitable for preventing phase transitions in NiTi strongly depends on the phase transformation temperature. The key findings of this research are as follows:

- DSC could be used to evaluate the critical phase transformation temperatures for SMAs. This information is useful in determining a machining strategy that would avoid temperatures for phase transformation.



**Fig. 13** Tool edge after machining with **a** chilled-air cutting and **b** dry cutting

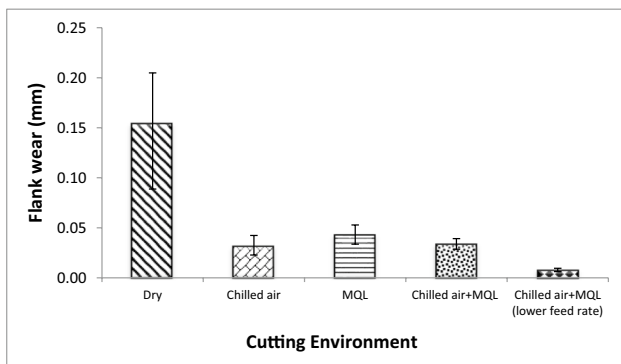
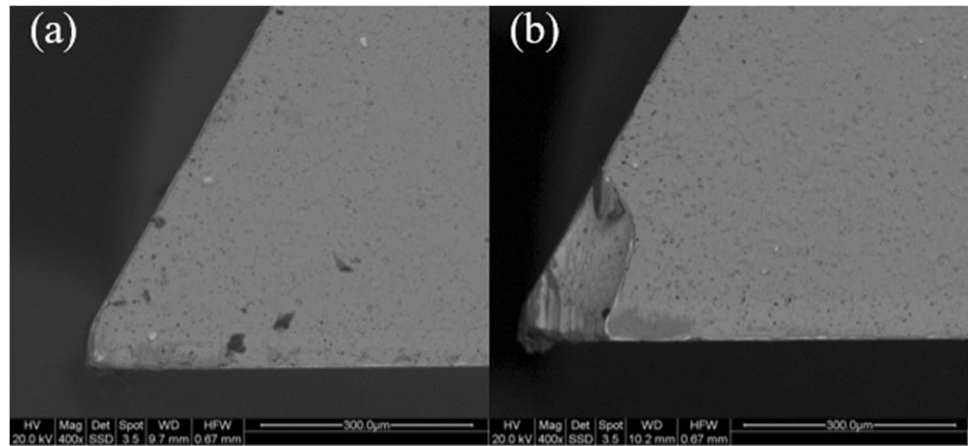


**Fig. 14** Tool wear dependence on cutting environment

- Compared to dry cutting, chilled air in machining significantly lowered the workpiece temperature to below the critical level for transformation to austenite, keeping the workpiece in the martensite phase. Note that the tool wear was reduced and more uniform.
- The machining process modified the temperature and duration for phase transformation from austenite to martensite. The resulting smaller thermal gradient for phase transformation can be exploited, enabling a faster actuation rate.
- As anticipated, dry cutting causes the subsurface's hardness to increase. This is a result of the large hone-cutting tool facilitating deeper and more compressive residual stress in the machined surface during dry cutting. Furthermore, it causes an increase in burr formation because the material is only pushed onto the slot side and not separated from the workpiece, resulting in burrs.
- The machining process also lowered the energy required for the austenite-to-martensite transformation. This opens up new opportunities to reduce the energy required for actuation, which may benefit industrial applications.
- The surface finish for SMAs was significantly improved (more than 50% reduction in surface roughness) by

simultaneous application of chilled air and MQL and exploiting the size effect using finer feed per tooth.

- This study contributes to the machining strategy of NiTi alloys (which begin to transform to austenite above room temperature and at 50 °C in the case presented). For materials with lower temperatures for the start of transformation to austenite, additional systems of more extreme cooling, such as cryogenic machining, can be considered.

**Funding** The first author gratefully acknowledges the financial funding of the government of Malaysia and University Malaysia Perlis. This research was funded and supported by Fundamental Research Grant Scheme (FRGS/1/2019/TK03/UNIMAP/03/2), Ministry of Higher Education, Malaysia.

**Data availability** Not applicable.

**Code availability** Not applicable.

## Declarations

**Ethics approval** Not applicable.

**Consent to participate** Not applicable.

**Consent for publication** The authors give full consent to the publisher for the publication of this work.

**Competing interests** The authors declare no competing interests.

**Open Access** This article is licensed under a Creative Commons Attribution 4.0 International License, which permits use, sharing, adaptation, distribution and reproduction in any medium or format, as long as you give appropriate credit to the original author(s) and the source, provide a link to the Creative Commons licence, and indicate if changes were made. The images or other third party material in this article are included in the article's Creative Commons licence, unless indicated otherwise in a credit line to the material. If material is not included in the article's Creative Commons licence and your intended use is not

permitted by statutory regulation or exceeds the permitted use, you will need to obtain permission directly from the copyright holder. To view a copy of this licence, visit <http://creativecommons.org/licenses/by/4.0/>.

## References

- Buehler WJ, Wang FE (1968) A summary of recent research on the nitinol alloys and their potential application in ocean engineering. *Ocean Eng* 1(1):105–120. [https://doi.org/10.1016/0029-8018\(68\)90019-X](https://doi.org/10.1016/0029-8018(68)90019-X)
- Jani JM, Leary M, Subic A, Gibson MA (2014) A review of shape memory alloy research, applications and opportunities. *Mater Des* 56:1078–1113. <https://doi.org/10.1016/j.matdes.2013.11.084>
- Liu Y (2010) Some factors affecting the transformation hysteresis in shape memory alloys. *Shape Memory Alloys*. Nova Science Publisher, Inc., pp 361–369
- Weinert K, Petzoldt V (2006) Machining NiTi micro-parts by micro-milling. *Mater Sci Eng, A* 481–482(2008):672–675. <https://doi.org/10.1016/j.msea.2006.10.220>
- Kaynak Y, Karaca HE, Noebe RD, Jawahir IS (2013) Tool-wear analysis in cryogenic machining of NiTi shape memory alloys: a comparison of tool-wear performance with dry and MQL machining. *Wear* 306(1–2):51–63. <https://doi.org/10.1016/j.wear.2013.05.011>
- Guo Y, Klink A, Fu C, Snyder L (2013) Machinability and surface integrity of Nitinol shape memory alloy. *CIRP Ann-Manuf Technol* 62(1):83–86. <https://doi.org/10.1016/j.cirp.2013.03.004>
- Wu SK, Lin HC, Chen CC (1999) A study on the machinability of a Ti 49.6 Ni 50.4 shape memory alloy. *Mater Lett* 40(July):27–32. [https://doi.org/10.1016/S0167-577X\(99\)00044-0](https://doi.org/10.1016/S0167-577X(99)00044-0)
- Weinert K, Petzoldt V (2004) Machining of NiTi based shape memory alloys. *Mater Sci Eng A* 378(1–2 SPEC. ISS.):180–184. <https://doi.org/10.1016/j.msea.2003.10.344>
- Piquard R, Acunto AD, Laheurte P, Dudzinski D (2014) Micro-end milling of NiTi biomedical alloys, burr formation and phase transformation. *Precis Eng* 38(2):356–364. <https://doi.org/10.1016/j.precisioneng.2013.11.006>
- Kaynak Y, Robertson SW, Karaca HE, Jawahir IS (2015) Progressive tool-wear in machining of room-temperature austenitic NiTi alloys: the influence of cooling/lubricating, melting, and heat treatment conditions. *J Mater Process Technol* 215:95–104. <https://doi.org/10.1016/j.jmatprotec.2014.07.015>
- Jawahir IS, Attia H, Biermann D, Dufflou J, Klocke F, Meyer D, Newman ST, Pusavec F, Putz M, Rech J, Schulze V, Umbrello D (2016) Cryogenic manufacturing processes. *CIRP Ann-Manuf Technol* 65(2):713–736. <https://doi.org/10.1016/j.cirp.2016.06.007>
- Kopac J (2009) Achievements of sustainable manufacturing by machining. *J Achiev Mater Manuf Eng* 34(2):180–187
- Abidin ZZ, Mativenga PT (2020) Harrison G. Chilled air system and size effect in micro-milling of nickel–titanium shape memory alloys. *Int J Precis Eng Manuf-Green Tech* 7:283–297. <https://doi.org/10.1007/s40684-019-00040-5>
- Bormann T, Friess S, Wild M, Schumacher R, Schulz G (2010) Determination of strain fields in porous shape memory alloys using micro computed tomography. *Proc SPIE* 7804(78041M):1–9. <https://doi.org/10.1117/12.861386>
- Mihalcz I (2001) Fundamental characteristics and design method for nickel-titanium shape memory alloy. *Periodica Polytechnica Ser Mech Eng* 45(1):75–86
- Kaynak Y, Karaca HE, Noebe RD, Jawahir IS (2013) Analysis of tool-wear and cutting force components in dry, preheated, and cryogenic machining of NiTi shape memory alloys. *Procedia CIRP* 8:498–503. <https://doi.org/10.1016/j.procir.2013.06.140>
- Biermann D, Kahleiss F, Surmann T (2009) Micromilling of NiTi shape-memory alloys with ball nose cutters. *Mater Manuf Processes* 24(12):1266–1273. <https://doi.org/10.1080/10426910903129935>
- American Society for Testing and Materials E112–96 (1999) Standard test method for determining average grain size. In *Annual Book of ASTM Standards*, pp 237–259

**Publisher's note** Springer Nature remains neutral with regard to jurisdictional claims in published maps and institutional affiliations.